[20]M. Rich, Phys. Letters 4, 153 (1963).
[21]E. J. W. Verwey *et al.*, Philips Res. Rept. 5, 173 (1950).
[22]R. R. Heikes and W. D. Johnson, J. Chem. Phys. 26, 582 (1957).
[23]G. M. Schwab and H. Schmid, J. Appl. Phys. Suppl. 33, 426 (1962).
[24]I. G. Austin, A. J. Springthorpe, and B. A. Smith, Phys. Letters 21, 20 (1966).
[25]A. J. Bosman and C. Crevecoeur, Phys. Rev. 144, 763 (1965).
[26]L. A. Kappers, R. L. Kroes, and E. B. Hensley, Phys. Rev. B 1, 4151 (1970).

PHYSICAL REVIEW B VOLUME 4, NUMBER 3 1 AUGUST 1971

Exchange Effects in the Optical-Absorption Spectrum of Fe^{3+} in Al_2O_3

J. J. Krebs and W. G. Maisch
Naval Research Laboratory, Washington, D. C. 20390
(Received 5 April 1971)

The polarized optical-absorption spectrum of Fe^{3+}-doped Al_2O_3 has been measured at room, liquid-nitrogen, and helium temperatures as a function of Fe^{3+} concentration (0.02–2 at.%). At low concentrations, the single-ion spectra are fit using the parameters $B=660$ cm^{-1}, $C/B=4.75$, and $Dq=1510$ cm^{-1}. At liquid-nitrogen temperature and above, there is a marked concentration dependence of the intensities of the $^4A_1$, $^4E^a$; $^4E^b$; and $^4T_1^b$ bands which indicates the importance of exchange enhancement. In particular, the $^4E^b$ band has a partially resolved component whose temperature and concentration dependence shows that it arises from exchange-coupled pairs of Fe^{3+} ions. The vanishing of this component at liquid-helium temperature indicates that it involves $\Delta S=0$ transitions analogous to those observed for Mn^{2+}. At 2% Fe^{3+}, the exchange-enhanced bands dominate the optical spectrum at room temperature, and one can anticipate a similar effect in most iron-rich oxides. Owing to the good (for Fe^{3+}) resolution obtained at 77 K, we are able to discuss some of the band details. A point-charge static odd crystal-field calculation of the electric dipole $^6A_1 \rightarrow {}^4A_1$ intensities is in very poor agreement with experiment, indicating the need to take lattice vibrations into account. Because of the existence of a strong spin-allowed Fe^{2+} transition in our samples, the two lowest-lying bands of Fe^{3+} in Al_2O_3 are not observed, but their positions are taken from the recent work of Lehmann and Harder.

INTRODUCTION

This paper is concerned with determining the low-temperature polarized optical spectra arising from Fe^{3+} ions in Al_2O_3 and establishing the importance of exchange-coupled pairs to the spectra observed for moderate ($\geq 0.5\%$) Fe^{3+} concentrations at 77 K and above. Quite reasonable values of the intraionic and cubic crystal-field parameters explain the observed spectra. The report also represents the discovery of a distinct exchange-coupled pair line in the optical spectrum of Fe^{3+}.

Until very recently, there has been a paucity of good data on the optical-absorption spectrum of trivalent iron. This fact is associated with the doubly (parity and spin) forbidden nature of transitions from the ^6S ground state of Fe^{3+} to any of the crystal-field-split quartet states. When the iron concentration is increased to overcome the inherent weakness of the Fe^{3+} bands, a strong absorption edge tends to mask all but the lowest-lying states. Further, the simultaneous existence of both octahedral and tetrahedral Fe^{3+} sites in many of the more interesting iron-bearing compounds has been a bar to interpreting the spectra found. Wickersheim and Lefever[1] reviewed the problem in 1962 and found an anomalous situation in which the technologically most important transition-metal ion had perhaps the most poorly understood energy-level scheme.

In 1967, Wood and Remeika,[2] in the process of examining the infrared optical window in yttrium iron garnet (YIG), were able to detect a substantial number of optical bands and successfully assign them to both octahedrally and tetrahedrally coordinated Fe^{3+}. By growing mixed gallium iron yttrium garnets, they were also able to determine the dependence of some of the band intensities on iron concentration and show that Beer's law is violated. More recently, the discovery that $FeBO_3$ and FeF_3 are transparent room-temperature canted antiferromagnets has stimulated study[3,4] of their optical and magneto-optical properties although no detailed band assignments exist as yet. The extensive work of Kahn *et al.*[5] on the rare-earth orthoferrites has altered the picture significantly. In this study, the ultraviolet region of the spectrum was examined using the complex polar Kerr effect. In particular, the nature of the strong absorptions which arise from parity and spin-allowed charge-

transfer transitions was determined. These are the bands which produce the absorption edge and normally obscure the short-wavelength region in Fe^{3+} optical studies. At the same time, these workers were able to detect a number of crystal-field transitions in the orthoferrites and make assignments.[5] Finally, Melamed *et al.*[6] have studied the fluorescence of Fe^{3+} in tetrahedral sites in ordered $LiAl_5O_8$ and assigned the observed transitions.

The principal purpose of the present work has been to examine the optical spectrum of Fe^{3+} in α-Al_2O_3 as a function of concentration and temperature in the hope of finding evidence for transitions involving exchange-coupled pairs of Fe^{3+} ions such as had already been found for pairs of the isoelectronic ion Mn^{2+}. Al_2O_3, which belongs[7] to the space group D_{3d}^6, possesses a number of useful properties for such a study.[8] First, it contains only octahedrally coordinated cation sites of a single type. This property is shared with the orthoferrites and produces an important simplification when making assignments. Second, the Fe^{3+} site in Al_2O_3 lacks inversion symmetry.[9] This means that the parity selection rule will be partially lifted by the odd components of the crystal field which mix states of odd parity into the even-parity ground manifold. Third, extensive work on the optical spectra of various $3d^n$ ions in Al_2O_3 has already been carried out by McClure.[8] This makes it possible to check whether a given band arises from some extraneous impurity. This is important for an ion such as Fe^{3+} which has inherently weak optical transitions. Finally, it is possible to grow good optical-quality Al_2O_3 crystals containing suitable amounts of Fe^{3+}. The use of a flux-growth method[10] enabled us to improve on the admittedly preliminary[8] results of McClure.

Although the present study represents the most detailed examination of the Al_2O_3:Fe^{3+} system to date, it is by no means the first. McClure's experimental work prompted Moorjani and McAvoy[11] to calculate the effect of crystal fields of trigonal symmetry on the splitting of the $3d^5$ cubic field states. Unfortunately, there are serious internal difficulties in the assignments which those authors made and compared with their calculations. Further, later work has not confirmed the very broad band at 18 200 cm^{-1} found by McClure. Townsend[12] examined the polarized spectrum of Al_2O_3 containing Fe^{3+} and saw a group of sharp lines in the 26 300-cm^{-1} region at 77 K. He correctly attributed these to Fe^{3+} but made no further analysis. In early 1970, Lehmann and Harder[13] published a study of the polarized room-temperature optical spectrum of natural corundum crystals containing iron as the major impurity. This work is the most closely related to the present one, and their assignments will be discussed later. It should be noted, however, that while their work gave a good value for the cubic crystal-field parameter $10Dq$, it did not indicate the important contribution of exchange-coupled Fe^{3+} pairs to the spectra they observed because no low-temperature data were taken.

In the present paper, we tend to emphasize those features of the data which illustrate the contribution of exchange effects to the Al_2O_3:Fe^{3+} optical spectra, including the observation of a resolvable band due to exchange-coupled pair transitions. However, the quality of the low-temperature data allows useful conclusions to be drawn about the details of the single-ion bands. The marked polarization behavior of certain band components is illustrated, and an attempt is made to explain these and other band details theoretically in terms of the combined effect of the noncubic components of the crystal field and the spin-orbit interaction. The interpretation of certain features observed by other workers[13] is also discussed.

THEORETICAL BACKGROUND

Although the behavior of the energy levels of a d^5 ion under the action of a cubic crystal field is well understood,[14] we review it briefly here for later reference and also calculate the effects of the spin-orbit interaction and of the trigonal crystal-field component in Al_2O_3. The selection rules and intensities of ${}^6A_1 \rightarrow {}^4A_1$ transition in C_{3v} and C_3 symmetry are discussed. Finally, we review the status of optical absorption from exchange-coupled pairs of paramagnetic ions.

Since in the $3d^5$ ions the d shell is half-filled, the opposing effects of the crystal field on d-shell electrons and holes forbid a linear crystal-field splitting of the energy levels of that configuration. As a result, for weak crystal fields, the energy levels exhibit a quadratic dependence on $10Dq$. This behavior is illustrated by the Tanabe and Sugano diagram[14] shown in Fig. 1. For the $10Dq$ values normally encountered in inorganic crystals, the high-spin ${}^6A_1$ state is the ground state. Because the ${}^4A_1$, ${}^4E^a$ band can usually be identified easily, the normalized energy-level scheme shown simplifies fitting. The strong-field matrix elements tabulated by Stevenson[15] were used in the calculations for Fig. 1 since they allow the introduction of the Tree's parameter α. In the final analysis, however, we found it convenient to take $\alpha = 0$ in order to maintain contact with previous work on Fe^{3+} optical spectra.

Probably the most complete discussion of spin-orbit effects for $3d^5$ ions has been given by Low and Rosengarten.[16] In their work, they diagonalized the complete cubic double-group Γ_6, Γ_7, and Γ_8 matrices. However, their results make it clear that the spin-orbit interaction has only a minor ef-

fect on the energies of the various states. Therefore, since the resolution obtained in the $Al_2O_3:Fe^{3+}$ spectrum does not justify an extensive calculation, the spin-orbit interaction was treated here as a perturbation. For a given $10Dq$ value, the states were expressed in the strong-field scheme and the diagonal spin-orbit terms were calculated using the matrix elements of Schroeder.[17] This procedure was checked against the exact calculations of Low and Rosengarten[16] and also Goode[18] and found to give satisfactory estimates of the splitting of various states. Table I lists the over-all splitting of the lower-lying Fe^{3+} energy levels calculated in this manner using $Dq = 1510$ cm^{-1} and $\zeta = 400$ cm^{-1}. (The spin-orbit parameter ζ has a free-ion value[19] of 420 cm^{-1}.)

To date, the only treatment of the trigonal-field splitting of the cubic states of a d^5 ion is that of Moorjani and McAvoy,[11] who use the weak-field scheme. Their matrix elements were checked and used here to calculate the splittings induced by the trigonal distortion in Al_2O_3. The various terms in the crystal-field potential expression of Ref. 11 were identified with the corresponding terms in McClure's expression[8] in order to recast the former work in terms of the more usual $10Dq$, and also

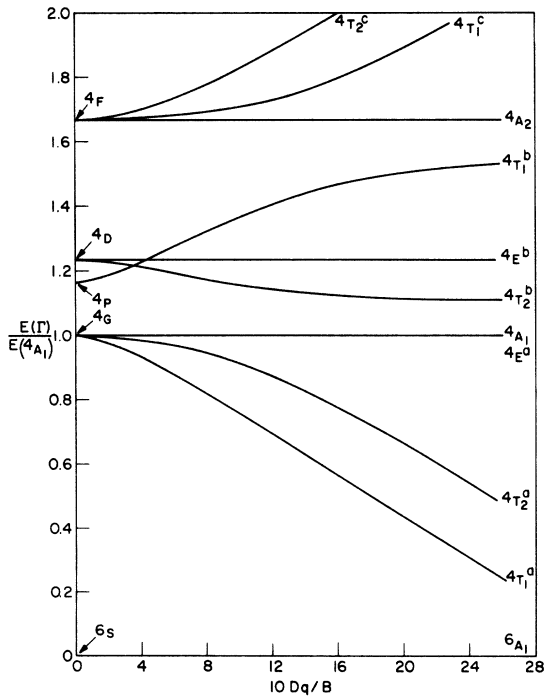

FIG. 1. Energy-level diagram for a $3d^5$ ion in a cubic crystal field. In this calculation, values $C/B = 4.75$ and $\alpha/B = 0.12$ were used. When the same cubic-field representation occurs more than once, it is labeled with an additional superscript (a, b, c), working upward from the lowest energy.

TABLE I. Spin-orbit and trigonal-field splitting of Fe^{3+} states in units of cm^{-1} ($Dq = 1510$ cm^{-1}, $B = 660$ cm^{-1}, $C/B = 4.75$).

State	Spin-orbit splitting[a]	Trigonal-field splitting $v(B_2^0)$	Trigonal-field splitting $v(\delta B_4^0)$
$^4T_1^a$	176	−299	−535
$^4T_2^a$	52	−614	−429
$^4A_1$, $^4E^a$	...	32	32
$^4T_2^b$	284	195	−104
$^4E^b$	...	...	...
$^4T_1^b$	271	−610	661
	($\zeta = 400$ cm^{-1})	($v = 1000$ cm^{-1})	

[a] Over-all splitting of outer components.
[b] E(singlet)−E(doublet).

v and v'—the trigonal-field parameters. According to McClure, the values of v and v' are given by

$$v = \tfrac{6}{7} B_2^0 \langle r^2 \rangle + \tfrac{160}{63} \delta B_4^0 \langle r^4 \rangle ,$$

$$v' = -\tfrac{2}{7}\sqrt{2}\, B_2^0 \langle r^2 \rangle + \tfrac{40}{63}\sqrt{2}\, \delta B_4^0 \langle r^4 \rangle ,$$

where δB_4^0 is the deviation of the Y_4^0-type crystal-field component from that required for a purely cubic field.[8] Furthermore, the B_l^m are related to the A_l^m of Ref. 11 by $B_2^0 = \frac{1}{4}(5/\pi)^{1/2} A_2^0$, $B_4^0 = \frac{3}{16}\pi^{-1/2} A_4^0$, and $B_4^3 = \frac{3}{4}(35/\pi)^{1/2} A_4^3$. In Table I we list the trigonal-field splitting of the lower-lying Fe^{3+} levels. Two extreme cases are considered, viz., v due entirely to B_2^0 or entirely to δB_4^0. None of the levels split perfectly linearly as a function of B_2^0 or δB_4^0, and for some states the splitting arising from $v(B_2^0)$ is opposite in sign to that from $v(\delta B_4^0)$. This is associated with the lack of diagonal crystal-field matrix elements. The value $v = 1000$ cm^{-1} is used in Table I since this is characteristic of that found[8,20] for various $3d^n$ ions in Al_2O_3. The values of the B, C, and Dq parameters used correspond to those necessary to give a good fit to the Fe^{3+} optical spectrum in Al_2O_3.

The selection rules forbid electric dipole transitions between states having the same parity, e.g., the same l^n configuration, and also between states of different spin. That means that no electric dipole transitions occur between the $^6A_{1g}$ ground state and the excited d^5 states of Fe^{3+} in the absence of interactions which break those restrictions. Spin-orbit interaction, the mechanism responsible for removing the spin restriction, has been thoroughly treated and applied to another d^5 ion, Mn^{2+}, by Englman.[21]

The parity restriction may be removed by the presence of odd fields which mix even states with odd states. Both static odd-crystal fields which exist in lower-symmetry environments (as in

TABLE II. Electric dipole selection rules for $^6A_1 \rightarrow {}^4A_1$ transition in C_{3v} and C_3 symmetries. Symbols: $\perp$, $\parallel$ mean $E\perp$, $\parallel c$ axis; ( ) means active in C_3 only. States are labelled in cubic-field double-group notation. See text for parity- and spin-breaking mechanisms.

		Γ_7			Γ_8		
$^4A_1$ \ $^6A_1$		$+\frac{1}{2}$	$-\frac{1}{2}$	$+\frac{3}{2}$	$+\frac{1}{2}$	$-\frac{1}{2}$	$-\frac{3}{2}$
Γ_8	$+\frac{3}{2}$	$\perp$	($\parallel$)	($\parallel$)	$\perp$		$\perp$
	$+\frac{1}{2}$		$\perp$	$\perp$	($\parallel$)	$\perp$	
	$-\frac{1}{2}$	$\perp$			$\perp$	($\parallel$)	$\perp$
	$-\frac{3}{2}$	($\parallel$)	$\perp$	$\perp$		$\perp$	($\parallel$)

Al_2O_3), or dynamic fields produced by odd vibrations (vibronic interaction), have been used to explain parity-forbidden transitions. The odd electronic states may be found in the higher excited configurations of the ion, e.g., $3d^{n-1}4p$ states of the iron group, or in states involving the surrounding ions, i.e., ligand-field states. Although McClure[8] considered the mixing of $4p$ states with the $3d$ states by the static crystal field, the contribution of such an interaction is expected to be small for Fe^{3+} since the lowest-lying $4p$ states are about 190 000 cm^{-1} above the ground level.[22]

Englman, in his treatment of Mn^{2+} in an octahedral environment,[21] assumed that the nearby charge-transfer states were the odd states which mixed with the $3d$ states. In his case, the centrosymmetric environment required that the odd fields be vibrational in origin. Because of the existence of low-lying, presumably charge-transfer, states of odd parity for Fe^{3+} in Al_2O_3,[23] we consider the possibility of mixing these ligand-field states with the $3d^5$ states by means of the odd static components of the trigonal field, and then calculate the selection rules and oscillator strengths of the resulting electric dipole transitions. The development of the electric-dipole-moment matrix elements for the strong-field states Γ is carried out in the Appendix. Selection rules for the $^6A_1 \rightarrow {}^4A_1$ transition in $\parallel$ and $\perp$ polarizations for various components of the odd crystalline field are given in Table II.

The real states of Fe^{3+} in Al_2O_3 are intermediate-field spin-orbit states, and it is these states which must be used if intensities between individual levels are to be calculated. Since the splitting of the $^6A_1$ ground state is small compared with the lowest experimental temperatures, it is reasonable to assume that the observed intensity of each band is merely the sum over all allowed transitions from every $^6A_1$ sublevel. Moreover, since the $^4A_1$ state is not mixed with the $^4E^a$ state by either spin-orbit interaction or the trigonal field, the $^6A_1 \rightarrow {}^4A_1$ band intensity may be obtained by a further summing over $^4A_1$ levels. The oscillator strength is defined as

$$f = (8\pi^2 mc/3he^2\lambda)\left|\langle \Gamma_e | P | \Gamma_g \rangle\right|^2$$

$$= 4.704 \times 10^{-29} \left| P \right|^2 \lambda^{-1} \text{ in cgs units,}$$

where the matrix elements are those calculated in the Appendix.

Beginning with the observation[24] of concentration-dependent sidebands on the R lines in ruby containing approximately 0.1–1.0-at.% Cr^{3+}, a wealth of literature has developed concerning electronic spectra arising from exchange-coupled pairs of magnetic ions. At moderate concentrations, the intensity of these optical lines is proportional to the square of the concentration. Such lines have been seen arising from Mn^{2+} pairs[25] in $KZnF_3$ and even from Mn^{2+}-Ni^{2+} pairs[26] in $KZnF_3$. Since they must be associated with narrow lines in order to be directly observed, the pair lines are normally found as satellites of transitions which involve spin flips only (same strong-field orbital configuration for the ground and excited states). Further, the oscillator strength of these pair lines is one or more orders of magnitude greater[27] than that of the corresponding single-ion lines. This gives rise to the anomalous intensity of some of the bands of $KMnF_3$ in comparison to $KZnF_3$:Mn^{2+}. It is important to note that spin-flip-only transitions referred to above exhibit a much greater over-all intensity enhancement due to pairs than transitions involving a change in orbital configuration.[27] This fact will prove useful in verifying our assignments. Finally, we note that in all of the above, only one ion of the exchange-coupled pair is excited at a time. The simultaneous excitation of both ions of the pair[28] was found to be important in the ultraviolet spectrum of $KZnF_3$:Mn^{2+}.

EXPERIMENTAL

Samples and Technique

The iron-doped Al_2O_3 crystals used in this work were obtained from two sources. Most were grown in our laboratory using a PbO-PbF_2 flux[10] to which iron was added in the form of Fe_2O_3. The nominal concentration of iron in the flux-grown samples used ranged from 0.1 to 2 at.%. Percentages in some of these samples were verified by x-ray-emission spectroscopy and wet chemical analysis. The crystals grow in the form of platelets with the broad face normal to the c axis and are typically 1 mm thick. All iron-doped crystals grown by this technique have a blue coloration which is frequently nonuniform within the crystal. Although the intensity of this color is roughly correlated with the iron content, we will show that it is not due to Fe^{3+}. In order to check on the presence of Fe^{2+} in the flux-grown crystals, the Mössbauer spectrum of a sample containing 2% Fe was run. Using the

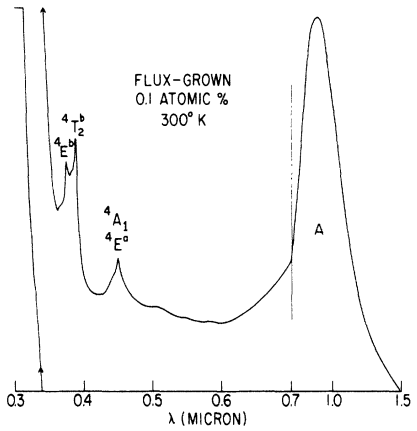

FIG. 2. Unpolarized room-temperature optical absorbance of a flux-grown Al_2O_3 crystal containing 0.1-at.% Fe^{3+}. Note the change in scale at 0.7 μm.

known[29] isomer shifts and quadrupole splittings of Fe^{2+} and Fe^{3+} in Al_2O_3, the fraction of iron in the divalent state was found to be 0.09, assuming the same Debye-Waller factor for both valence states.

Additional crystals, grown by the flame-fusion technique, were obtained[30] to try to eliminate some interfering absorption bands found in the flux-grown crystals. Based on the spectral and visual examination of the flame-fusion crystals, it appears difficult to introduce more than approximately 0.1% Fe^{3+}. At higher initial iron levels, a large fraction of the Fe_2O_3 does not dissolve in Al_2O_3 but forms bubbles in the crystals, presumably due to the high vapor pressure of Fe_2O_3 at the melting point of Al_2O_3.

The optical-absorption spectra were obtained in the wavelength range 0.3–1.5 μm using a Cary model 14R spectrophotometer. Samples were cut and mounted in a variable-temperature Sulfrian Dewar so that $E \parallel C$ (π polarization) and $E \perp c$ (σ polarization) spectra could be taken by merely orienting external polarizers in the sample and reference beams. In a few cases, spectra were taken for light propagation along the c axis.

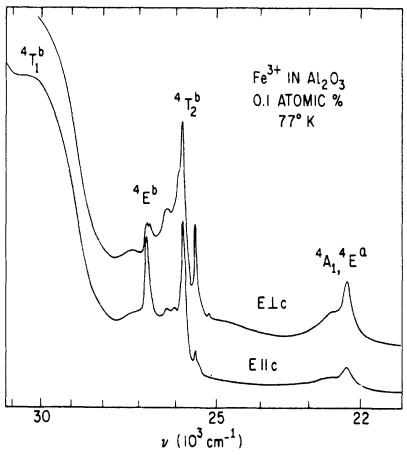

FIG. 3. Polarized optical absorbance (plotted in arbitrary units) at 77 K versus energy ν for the same sample as in Fig. 1.

Low-Concentration Results

A general view of the unpolarized room-temperature spectrum for a low-concentration (0.1%) sample is shown in Fig. 2. The length of the sample was 1.9 cm. The broad, intense band in the 0.9-μm region (band A) is not due to Fe^{3+} but is shown for completeness. In Fig. 3, we show the $E \parallel c$ and $E \perp c$ spectra of the same low-concentration sample at liquid-nitrogen temperature. Bands near 22 000 cm^{-1} and in the 25 000–27 000 cm^{-1} region both show structure at this temperature. Our band assignments are indicated in Figs. 2 and 3. The reasons for these assignments, which agree with those of Lehmann and Harder,[13] will be given later. A number of features show significant dichroism, in particular, the sharp lines at 25 500 and 26 800 cm^{-1}.

The positions of the various components of the $^4A_1$, $^4E^a$, the $^4T_2^b$, and the $^4E^b$ bands are listed in Table III. Most of these are easily identifiable with features in Fig. 3. One point which should be stressed is that the components marked with a subscript b are no longer present when the temperature is reduced to 15 K. Except for this, the components may be considered as those characteristic of the isolated Fe^{3+} ion in Al_2O_3.

Concentration-Dependent Results

The strong effect of concentration on the appear-

TABLE III. Position of Fe^{3+} absorption-band components in Al_2O_3 at 77 K (in units of cm^{-1}). Concentration: 0.1 at.%.

Band	$E \perp c$	$E \parallel c$
$^6A_1 \rightarrow$		
$^4A_1$, $^4E^a$	22270	22270
	22540[a]	22570[a]
$^4T_2^b$	25180	
	25410[a]	25410[a]
	25520	25510
	25840	25820
	25930[a]	
		26030
	26240	26230
$^4E^b$	26680[b]	26660[a,b]
	26770	26780
		26980[c]
	27210[c]	27170[c]

[a] Shoulder. [b] Absent at 15 K. [c] Position uncertain.

ance of the $^4A_1$, $^4E^a$ band is illustrated in Fig. 4 for $E \perp c$. The concentration-length product for these samples is approximately constant so that a direct comparison of the spectra is possible. The large enhancement of the band intensity of the 2% sample at room temperature almost vanishes at liquid-helium temperature (actually 13 K). The concentration and temperature dependence of the $^4E^b$ and $^4T_2^b$ bands is indicated in Fig. 5. The spectrum labelled A (0.5% and 77 K) is directly comparable with the 0.1% $E \perp c$ spectrum shown in Fig. 3. Note the marked enhancement of the lower-energy component of the $^4E^b$ band at this concentration. When the temperature is reduced into the liquid-helium range, the 0.5% (trace B) and 0.1% (trace C) spectra become almost identical. A slight residual shoulder can still be noted at the $^4E^b$ band for the more concentrated sample, however. Figure 5 makes it obvious that the $^4T_2^b$ band does not partake in the unusual concentration and temperature behavior. The spectra clearly imply that the enhanced high-temperature absorption in the $^4A_1$, $^4E^a$ and the $^4E^b$ bands at higher concentrations arises from states which are thermally depopulated at liquid-helium temperatures.

Since we find that the peak absorbance of the $^4T_2^b$ band follows Beer's law quite well, it serves as a convenient measure of the Fe^{3+} concentration when surveying a number of crystals. We define the quantity $\alpha = l^{-1} \log_{10}(I_0/I)$, where l is the sample length in cm, and I_0 and I are the incident and transmitted light intensities. Figure 6 shows a plot of $\alpha(^4A_1, {}^4E^a)$ and $\alpha(^4T_1^b)$ vs $\alpha(^4T_2^b)$ for a number of flux- and flame-fusion-grown samples. The data were taken at room temperature and represent unpolarized spectra. The most important feature from our point of view is the nonlinear dependence

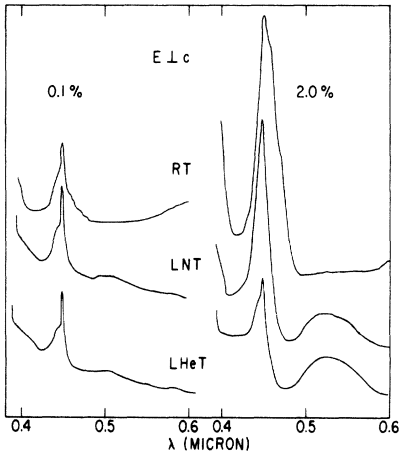

FIG. 4. Effect of concentration and temperature on the $^4A_1$, $^4E^a$ band of Fe^{3+} in Al_2O_3.

FIG. 5. Effect of concentration and temperature on the $^4E^b$ and $^4T_2^b$ bands of Fe^{3+} in Al_2O_3. Trace A, 0.5% Fe^{3+}, liquid-nitrogen temperature; trace B, 0.5%, liquid-helium temperature; trace C, 0.1%, liquid-helium temperature. The vertical scale is the optical absorbance in arbitrary units while ν is the photon energy.

of $\alpha(^4T_1^b)$ and $\alpha(^4A_1, {}^4E^a)$ on concentration. The data in Figs. 4–6 provide the primary evidence for exchange-enhanced band intensities for Fe^{3+} in Al_2O_3. They will be discussed in more detail later.

In order to convince ourselves that none of the effects observed were artifacts of the growth process and perhaps not due to Fe^{3+}, flame-fusion samples of Al_2O_3:Fe were also examined. By using a triple pass through an Al_2O_3 crystal 5.35 cm long, good room-temperature spectra were obtained at very low Fe^{3+} concentration (< 0.02%). In this sample, the broad band at 0.9 μm was much weaker than in the flux-grown samples. However, the other details of the spectra were unchanged.

The oscillator strengths f of a number of selected transitions were measured at 77 K. The results of

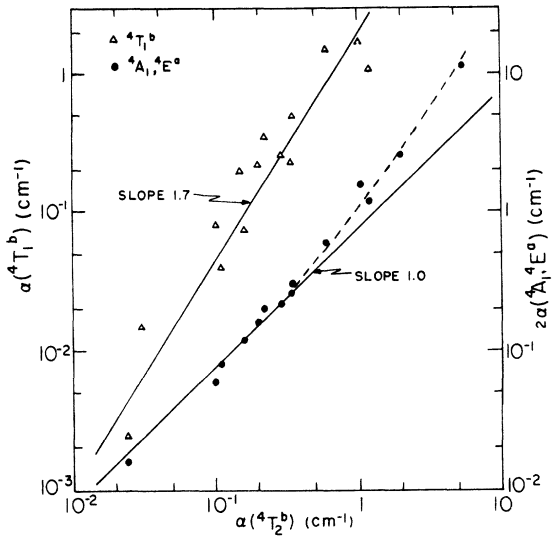

FIG. 6. Dependence of $\alpha(^4A_1, {}^4E^a)$ and $\alpha(E^b)$ on concentration at room temperature. [$\alpha(^4T_2^b)$ is proportional to the concentration.] The quantity $\alpha = l^{-1} \log_{10}(I_0/I)$.

these measurements are summarized in Table IV. The absolute f numbers may be in error by a factor of 2 owing to concentration and measurement uncertainties. However, the increase in f for the $^4A_1$, $^4E^a$ band with increasing concentration is real. This effect is even more apparent in the room-temperature absorption spectra as can be seen in Fig. 4.

DISCUSSION

In this section, we consider the question of assignments, the role of exchange-coupled pairs at higher Fe^{3+} concentrations, band details, including polarization in relation to selection rules, and finally the origin of the band at 0.9 μm.

Assignments

The question of assignments is not as clear as it might appear at first sight. A general rule of thumb has been to assign the sharp bands observed in $3d^5$ spectra to transitions from $^6A_1$ to $^4A_1$, $^4E^a$ and/or $^4E^b$. This is based on the fact that these transitions are crystal field independent (Fig. 1)

TABLE IV. Oscillator strengths ($f \times 10^6$) of selected optical transitions of Fe^{3+} in Al_2O_3, at 77 K.

Fe^{3+} Concentration (at.%)	$^4A_1$, $^4E^a$		$^4T_2^b + {}^4E^b$	
	$E \parallel c$	$E \perp c$	$E \parallel c$	$E \perp c$
0.1	1.0	2.2	7.6	11.3
0.5	2.8	4.4	...	...
1.0	6.5	7.6	...	...
2.0	15.0	14.0	10.4	12.8

TABLE V. Room-temperature optical spectrum of natural iron-bearing corundum crystals (as taken from Ref. 13), in units of cm^{-1}.

Band	Energy	Band	Energy
$^4T_1^a$	9450	$^4T_2^b$	25 680
$^4T_2^a$	14 350	$^4E^b$	26 570
(split)	17 600	$^4T_1^b$	29 000
$^4A_1$, $^4E^a$	22 120		

and hence should be rather sharp even at room temperature. Following this dictum, the $^4A_1$, $^4E^a$ and $^4E^b$ bands are identified with the 22 270-cm and 26 800-cm^{-1} bands, respectively. Once these two transitions are pinned down, $10Dq$ can be determined from the location of the $^4T_1^a$ or $^4T_2^a$ band. Unfortunately, in all the samples examined in this study, the portion of the spectrum where these latter bands should appear is masked by band A near 0.9 μm (11 300 cm^{-1}). Although various samples exhibited other weak bands which could be observed when band A narrowed at low temperatures, these were not consistent from sample to sample. Band A was weakest in flame-fusion-grown crystals but, since the Fe^{3+} content was also quite low in these samples, no $^4T_1^a$ or $^4T_2^a$ band could be identified with certainty. This illustrates the difficulty of measuring inherently weak spectra such as that due to Fe^{3+}, since small amounts of an impurity such as Fe^{2+} or Cr^{3+}, which have spin-allowed transitions, can distort the observed spectrum considerably. Transitions to $^4T_2^b$ are nearly independent of $10Dq$ at reasonable values of this parameter (Fig. 1) which leaves $^4T_1^b$ to determine $10Dq$. It is rather distressing that no acceptable value of $10Dq$ can expain the rather low value found, viz., $E(^4T_1^b)/E(^4A_1) = 1.34$. Thus either the $^4T_1^b$ assignment is incorrect or one must invoke additional interactions, such as the configuration interaction, to explain the depressed location of this state.

Fortunately, while this work was being prepared for publication, the study of Lehmann and Harder[13] on the optical spectrum of natural iron-bearing corundum crystals appeared. Their findings are summarized in Table V. Their assignments for the $^4A_1$, $^4E^a$ band and bands at higher energies agree with those given here. However, they were able to find several bands at lower energies in crystals which did not contain band A. We question their assignment of the band at 17 600 cm^{-1} and attribute it to a small amount of Cr^{3+} impurity in their samples. This agrees with the location and polarization behavior of this band.[8] The corresponding Cr^{3+} band near 25 000 cm^{-1} would be hidden under the $^4T_2^b$ and $^4E^b$ bands. We found direct evidence of

TABLE VI. Optical-absorption spectra of Fe^{3+} in octahedral surroundings, in units of 10^3 cm^{-1}.

Band	FeF_3[a]	$FeBO_3$[b]	YIG[c]	$ErFeO_3$[d,e]	Al_2O_3[f]	Calc[g]
$^4T_1^a$	16.5	11.2	10.2 11.1	10.0	9.45	9.72
$^4T_2^a$	21.8	16.6	14.3	14.3	14.35	14.16
$^4A_1, ^4E^a$	26.8	...	...	19.0	22.27	22.27
$^4T_2^b$	29.6	...	...	21.6	25.51	24.53
$^4E^b$	31.8	...	...	...	26.8	26.9
$^4T_1^b$	37.0	...	...	29.0	29.8	33.5

[a] Reference 4, our interpretation.
[b] Reference 3, our interpretation.
[c] Reference 2.
[d] Reference 5.
[e] D. L. Wood, L. M. Holmes, and J. P. Remeika, Phys. Rev. 185, 689 (1969).
[f] Reference 13 and this work.
[g] Using $B = 660$ cm^{-1}, $C/B = 4.75$, and $Dq = 1510$ cm^{-1}.

such contamination in a flame-fusion crystal used in this study and, more tellingly, found no evidence of a 17 600-cm^{-1} band in our flux-grown samples of $Al_2O_3:Fe^{3+}$. Finally, assigning[13] the 17 600- and 14 350-cm^{-1} bands as split components of $^4T_2^a$ gives an untenably large splitting as Table I shows.

Let us now consider the two remaining bands of Lehmann and Harder. There is no common trivalent transition-metal impurity other than Fe^{3+} which would explain these bands.[8] In Table VI, we list the location of Fe^{3+} optical bands found in several octahedrally coordinated iron-containing compounds and compare them to $Al_2O_3:Fe^{3+}$. It is apparent from the data on $ErFeO_3$ and YIG that the Lehmann and Harder assignments of the 9450- and 14 350-cm^{-1} bands are quite reasonable, and we accept them as correct. Using the above assignments, we obtain the fit shown in the last column of Table VI using $B = 660$ cm^{-1}, $C/B = 4.75$, and $Dq = 1510$ cm^{-1}. These values are all quite in keeping with expectations for a trivalent ion in octahedral oxygen surroundings.[31] The reason for the small disagreement with the $Dq = 1440$-cm^{-1} value of Ref. 13 is not clear, and the previously mentioned problem of the $^4T_1^b$ state remains quite evident. However, all of the other states agree rather well with this calculation.

Exchange-Coupled Fe^{3+} Pairs

We have already pointed out the anomalous concentration and temperature dependence of the $^4A_1$, $^4E^a$ and $^4E^b$ bands in Fe^{3+}-doped Al_2O_3 and now give an explanation of these data in terms of exchange-coupled pairs of Fe^{3+} ions. The concentration dependence shown in Figs. 3–6 and Table IV indicates that Beer's law breaks down and the absorption in these bands is increasing more rapidly than the Fe^{3+} concentration c, at least at the higher concentrations. This is in accord with the experience in $KMnF_3$ for which[25] the intensity of these same bands is abnormally large in comparison to $KZnF_3:Mn^{2+}$. Since the $^4E^b$ band is the most instructive, it will be discussed first.

At sufficiently low concentrations and temperatures, the $^4E^b$ band consists of a single component located at 26 790 cm^{-1} in both polarizations. It is relatively weak in the $E \perp c$ polarization. At temperatures below 13 K, the $^4E^b$-band oscillator strength is almost independent of concentration (Fig. 5, traces B and C). However, at 77 K, although phonon effects are still not significant in Al_2O_3, there is a strong concentration dependence. This effect is even more impressive in samples with $c > 0.5\%$, but the encroaching edge of the $^4T_1^b$ band makes display difficult. The principal change at 77 K is the growth of a new band component centered on 26 670 cm^{-1} which is not significantly polarized. (The exact polarization behavior is difficult to determine because of overlap with the 26 790-cm^{-1} component.) We associate this new band component with transitions involving exchange-coupled Fe^{3+} pairs although the 26 790-cm^{-1} component clearly has a single-ion origin. The intensity of the new component is best measured in the $E \perp c$ polarization for which there is the least interference with the single-ion line. Measurements show that the peak absorbance α is proportional to $c^{1.8\pm0.2}$ at 77 K. At 300 K, the effect of concentration on the $^4E^b$ band is easily noted in both polarizations, but line broadening makes detailed analysis impossible.

The unusual temperature dependence suggests that the new transition originates from a state which is thermally depopulated at $T = 0$. Since the component is not present at Fe^{3+} concentrations which are sufficiently low, phonon effects are ruled out. However, both the concentration and temperature characteristics are easily explained in terms of transitions involving exchange-coupled pairs of Fe^{3+} ions in which one member of the pair is excited to the $^4E^b$ state while the other member remains in the $^6A_1$ ground state. On the basis of previous work,[27] the selection rule $\Delta S = 0$ is known to be rather well satisfied for such pairs. Here S is the spin quantum number which characterizes the exchange-coupled states of the pair. Figure 7 indicates the allowed transitions as well as the possible values of S in the ground and excited states of the pair. This level scheme assumes that the pair interaction has the simple form $\mathcal{H}_{ex} = J\vec{S}_a \cdot \vec{S}_b$ and hence the energy is given by

$$E_g = \tfrac{1}{2}J[S(S+1) - S_a(S_a+1) - S_b(S_b+1)] \quad (1)$$

in the ground state with $S_a = S_b = \frac{5}{2}$, $S = 0, 1 \ldots, 5$;

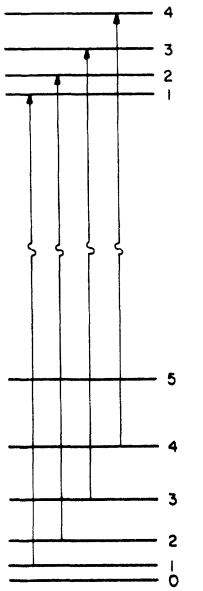

FIG. 7. Schematic presentations of the ground and excited states of a Fe^{3+}-Fe^{3+} exchange-coupled pair. The allowed ($\Delta S = 0$) transitions are shown.

while in the excited state $S_a = \frac{5}{2}$, $S_b = \frac{3}{2}$, $S = 1$, 2, 3, 4, and we replace J by K. There is evidence[27] that Eq. (1) is not completely accurate, but it is adequate for our qualitative purposes.

The origin of the temperature dependence of the new band component is then quite clear. As the sample is cooled, the upper levels of the pair ground state depopulate thermally, and at sufficiently low temperatures only the $S = 0$ ($S = 5$) level is populated if $J > 0$ ($J < 0$). In either case, there is no allowed pair transition and only the single-ion transition is seen in this region of the spectrum. The concentration dependence arises, of course, from the fact that for small c the number of pairs, assuming a random distribution of Fe^{3+}, is proportional to c^2 rather than c. While it is tempting to try to relate the 120 ± 20-cm^{-1} spacing between the $^4E^b$ single-ion component and the corresponding pair component to J and K, one must remember that local lattice distortions induced by the nearby Fe^{3+} pair member make any such calculation dubious. A detailed temperature dependence of the pair line intensity should allow the sign and value of J to be determined. Such measurements are in progress and will be reported at a later date. However, the depopulation of the upper levels at $T = 13$ K and other data suggest that $|J|$ is of the order of 20 K if $J > 0$ and less if $J < 0$. Hence it would appear that these are not nearest-neighbor pairs.

The data of Fig. 6 show that the room-temperature intensity of the $^4A_1$, $^4E^a$ band is in fact proportional to concentration at low concentrations but when $\alpha(^4T_2^b)$ exceeds 0.5 cm^{-1}, the intensity increases anomalously. This corresponds to Fe^{3+} concentrations of 0.5% or greater. At the highest Fe^{3+} concentration investigated here (2%), one finds that $\alpha(^4A_1, ^4E^a)$ is proportional to $c^{1.7}$. Further, as Fig. 4 shows, this band also has a strong dependence on temperature at higher concentrations even though this is absent for $c \leq 0.2\%$. This is interpreted as meaning that pair transitions are also appearing as satellites of the $^4A_1$, $^4E^a$ band with increasing concentration but that they are unresolved due to the larger width of this band. This interpretation is further supported for higher-concentration samples by an anomalously large red shift (≥ 50 cm^{-1}) of their band peak as the temperature is raised to 300 K.

It is worth noting that Wood and Remeika[2] found that the absorbance of the octahedral and tetrahedral $^4T_1^a$ bands of Fe^{3+} in $Y_3(Fe_cGa_{1-c})_5O_{12}$ varied as $c^{1.8}$ over the range $0.03 \leq c \leq 1.0$. They were unable to decide whether this was due to intensity borrowing from the states which produce the absorption edge they observed or to some spin-spin interaction which helped lift the spin selection rule. The observation of a resolved pair line in Al_2O_3:Fe^{3+} suggests that the latter is the case.

No anomalous behavior is found in the $^4T_2^b$ band at any temperature or Fe^{3+} concentration. This is in agreement with the lack of significant pair enhancement of the intensity of this band in $KMnF_3$, for example.[27] It should be noted that the behavior of the three bands just discussed helps verify their assignments by analogy with $KMnF_3$ and $KZnF_3$:Mn^{2+}.

As far as the remaining $^4T_1^b$ band is concerned, we have already indicated the marked concentration dependence of the room-temperature peak absorbance in Fig. 6. As can be seen, $\alpha(^4T_1^b)$ is proportional to $c^{1.7}$ although there is considerable scatter in the data, partly due to the encroaching absorption edge at higher concentrations. This finding suggests that the $^4T_1^b$ transition is exchange enhanced. Another possible assignment for the 29 800-cm^{-1} band should be noted in passing. That is, it could arise from the simultaneous excitation of both members of an exchange-coupled pair from their $^6A_1$ ground states to their $^4T_2^a$ excited states. This would be consistent with the concentration dependence and with the finding that this band does not disappear at low temperatures since, if the exchange constant were positive, the $S = 0$ level involved in the now possible $0 \rightarrow 0$ transition would still be populated. Similar double excitations have been found[28] in $KMnF_3$ (although not involving $^4T_2^a$ only). The principal argument against this assignment is the fact that $2 \times 14\,350$ $cm^{-1} = 28\,700$ cm^{-1}, not the 29 800 cm^{-1} found. In the case of $KMnF_3$, the match is much more nearly exact. As a result, further speculation on such an assignment does not seem fruitful.

Band Details

Working upward in energy, we consider the $^4A_1$, $^4E^a$ band first. Two components are found (Table III) separated by approximately 280 cm^{-1}. The question is: Which is the $^4E^a$ transition? First, we consider what light the calculated f numbers can throw on this question. In order to calculate $f(\parallel)$ and $f(\perp)$ for the $^6A_1 \rightarrow {}^4A_1$ transition, the following values are used in Eqs. (A8) and (A9) of the Appendix: $\zeta = 400$, $\Delta(^6A_1, {}^4T_1^a) = 10^4$, $\Delta(^4A_1, {}^4T_1^b) = 3\times10^4$, all in units of cm^{-1}; $\langle r^n \rangle = S(\alpha R_0)^n$, where $S(=0.1)$ is an overlap integral. $R_0(=2$ Å) is the metal-ligand distance and $0.5 \le \alpha \le 0.7$. Furthermore, the crystal-field sums,[32] in units of eV (Å)$^{-n}$ for B_n^l, are $B_1^0 = 0.82$, $B_3^0 = -0.60$, $B_3^3 = -1.52$, and $C_3^3 = 0.088$.

The results of these calculations, however, are in substantial disagreement with experiment. First of all, the ratio $f(\parallel)/f(\perp)$ is predicted to be roughly

$$\left| C_3^3/(\sqrt{2}\, B_3^0 + B_3^3) \right|^2 \approx 1.7\times10^{-3}$$

for $^6A_1 \rightarrow {}^4A_1$. There is no such strongly polarized component in the $^4A_1$, $^4E^a$ band. Second, the predicted absolute intensities are far too small [$\le 3\times10^{-8}$ for $f(\perp)$ in comparison with 2.2×10^{-6} found for the combined band]. Note that according to Table II, $f(\parallel)$ would vanish in C_{3v} symmetry. Its predicted small size is due to the rather slight deviation of the symmetry from C_{3v} in Al_2O_3. (Compare C_3^3, which is forbidden in C_{3v}, and B_3^3.) The $\langle r^n \rangle$ estimates used are open to considerable error but, when taken in conjunction with the B_n^l used, values larger than our upper limit do not seem physically reasonable [e.g., $\langle {}^4A_1 \| V(T_{1u}) \| {}^4T_1^l \rangle \approx 5000$ cm^{-1}]. Parenthetically, we note that if the odd $3d^4 4p$ states are used instead of the ligand-field states, a strong polarization of $^6A_1 \rightarrow {}^4A_1$ is still predicted, in contrast with experiment. It thus appears that a calculation based on the static odd crystal-field components alone is inadequate.

The polarization properties point to the importance of considering the $^6A_1 \rightarrow {}^4A_1$ transition as vibrationally assisted. Our observation, especially for $E \parallel c$, of a nontrivial temperature dependence of the intensity of this band at low Fe^{3+} concentration also suggests the importance of vibrational modes. The odd lattice vibrations have two distinct effects. First, they provide a parity lifting mechanism as noted above. In the case of $Mn(H_2O)_6^{2+}$, Englman[21] has shown that this mechanism predicts $f \simeq 2\times10^{-7}$ for the band under consideration, still an order of magnitude smaller than that found experimentally. Second, the odd vibrational modes, since their representations are not so restrictive as the static odd fields, can be expected to result in a much larger $f(\parallel)/f(\perp)$ ratio. It is possible, of course, that there is still an appreciable exchange enhancement of this band intensity at 0.1-at.% Fe^{3+} although the low-concentration behavior shown in Fig. 6 tends to refute this. We have chosen not to pursue the problem of vibrationally assisted intensities in detail.

Let us return more specifically to the locations of the $^4E^a$ transition. In treating the related problem for Mn^{2+} in various fluoride hosts, Ferguson[28] and Ferguson *et al.*[25] have argued that the $^4E^a$ level lies approximately 140 cm^{-1} below $^4A_1$. Since this is opposed to the theoretical ideas of Koide and Pryce,[33] Ferguson[28] shows that the experimental order can be reproduced by allowing greater covalency in the $^4E^b$ state than in the interacting $^4E^a$ state. The most convincing argument offered for their assignments is the splitting of the $^4E^a$ band in $KMnF_3$ below 60 K. No such helpful splitting occurs in the Al_2O_3:Fe^{3+} system because of the C_3 symmetry. Nevertheless, we assign $^4E^a$ to the lower of the two band components in agreement with Ferguson's Mn^{2+} arguments. We note, however, that the actual splitting is much larger than Table I predicts and hence must be enhanced by other mechanisms such as Ferguson's suggestion or perhaps a larger value for v and v'. As a result, the assignment is tentative.

Moving now to the $^4T_2^b$ band, we note that (i) it is resolved into at least eight components, (ii) the components are relatively sharp, and (iii) below 77 K the band is largely independent of temperature and concentration. From Table I we expect a spin-orbit splitting of 280 cm^{-1} and a trigonal-field splitting of 200 cm^{-1} or less. Under the combined action of these two interactions, $^4T_2^b$ will be split into six Kramer's doublets which will be separated by less than 500 cm^{-1} for $v = 1000$ cm^{-1}. Hence, we can conclude that some of the components found for the $^4T_2^b$ band (Table III) must be phonon assisted.

The known infrared[34] and Raman[35] active vibrational modes cluster near the energies 420, 580, 640, and 750 cm^{-1}. If one takes the components at 25 180, 25 410, and 25 510 cm^{-1} as being band origins for transitions to various components of the split $^4T_2^b$ state, then the rest of the components can be matched within 30 cm^{-1} by adding one of the phonon energies listed above. (A mismatch of 30 cm^{-1} is considerably less than a linewidth.) From the above considerations, we suggest that aside from the lowest three components, the rest of the observed $^4T_2^b$ band is due to phonon-assisted transitions.

As to why the components are sharp, we refer to Fig. 1. For $10Dq/B \approx 20$, as is true for Fe^{3+} in Al_2O_3, the energy difference $E(^4T_2^b) - E(^6A_1)$ is nearly independent of $10Dq$. This in itself will lead to fairly sharp lines. A more careful examination of the reason for this lack of dependence on the cubic field shows that for this value of $10Dq/B$ the

$^4T_2^b$ state is 94% $t_2^3e^2$. The ground state, of course, is pure $t_2^3e^2$. This means that a $^6A_1 \rightarrow {}^4T_2^b$ transition should excite relatively few Al_2O_3 vibrational modes. This is especially true because of the rather high energy (≥ 380 cm^{-1}) of these modes. The result is a well-defined spectrum.

As noted earlier, the only transitions which are exchange enhanced are those involving spin flips only in the strong-field notation. The absence of any concentration-dependent effects for the $^4T_2^b$ band shows how strong this requirement really is. Even though $^4T_2^b$ is largely derived from the same strong-field configuration as $^6A_1$, there are no exchange effects. Thus the case of Fe^{3+} in Al_2O_3 is a much stronger argument for the necessity of spin-flip-only transitions, if one is to see significant amounts of exchange enhancement, than is the case of the Mn^{2+} fluorides, since the Fe^{3+} $^4T_2^b$ state is much more nearly pure $t_2^3e^2$ than is Mn^{2+}.

Finally, for $^4E^b$ we find just a single component at low temperatures and concentrations. This is in agreement with Table I which shows that there is no trigonal or first-order spin-orbit splitting expected in this state. As expected, the assigned $^4T_1^b$ state is fairly broad since it is dependent on $10Dq$.

Band A

A few comments concerning this band are in order. Although the band is responsible for the blue coloration observed and its intensity is roughly correlated with the iron concentration of various flux-grown samples, two facts lead to eliminating an Fe^{3+} origin for band A. First, substantial changes in the band-A intensity from place to place in a given crystal were noted, even though the $^4T_2^b$ band of Fe^{3+} showed negligible fluctuation. Second, band A is very weak in flame-fusion-grown samples examined in this work and apparently absent in some iron-containing natural Al_2O_3 crystals.[13] As a result, we agree with the conclusion of Lehmann and Harder that this band is due to Fe^{2+}. Further, if we take the fraction of iron present as Fe^{2+} to be 0.09, as the Mössbauer results suggest, we obtain an unpolarized f number of 1.3×10^{-3} for band A in good agreement with their value.[13] It is well known[36] that the use of PbO-PbF_2 flux leads to the inclusion of small amounts of fluorine ions in the Al_2O_3 crystals grown. In replacing oxygen, the fluorine presumably acts as a charge compensator. A small concentration of Fe^{2+} is sufficient since the $^5T_2 \rightarrow {}^5E$ transition involved is spin-allowed.

In contrast with the work of Ref. 13, however, no band in the 15 600–16 400-cm^{-1} region was found in our samples containing band A. Hence, the assignment of such a band to Fe^{2+} in Al_2O_3 must be incorrect. This finding results in the apparent absence of any resolved Jahn-Teller splitting of the $^5T_2 \rightarrow {}^5E$ band of Fe^{2+} in Al_2O_3. At low temperatures, there is some narrowing of band A, but no new details emerge aside from the fact that for $E \perp c$ the peak is 200–300 cm^{-1} higher in energy than for $E \parallel c$.

SUMMARY

An examination of the temperature and concentration dependence of the optical-absorption spectra of Fe^{3+} in Al_2O_3 indicates that the exchange interaction plays an important role in the intensity of the $^4A_1$, $^4E^a$ and the $^4E^b$ bands. In the latter case a component arising from exchange-coupled pairs of Fe^{3+} ions has been identified. Such effects are not expected to be limited to the Al_2O_3:Fe^{3+} system alone, but rather, all iron-rich oxides (e.g., spinels, garnets, orthoferrites) should have their corresponding bands strongly exchange enhanced.

The optical-absorption spectrum of the isolated Fe^{3+} ion in Al_2O_3 found here agrees with the room-temperature results of Lehmann and Harder[13] on natural crystals and is characterized by the parameters $B = 660$ cm^{-1}, $C/B = 4.75$, $Dq = 1510$ cm^{-1}. On the basis of the estimated spin-orbit and trigonal-field splitting of the $^4T_2^b$ band, a number of observed low-temperature components are attributed to simultaneous vibronic and electronic excitations. An attempt to calculate the absorption intensity of the $^6A_1 \rightarrow {}^4A_1$ transition based on point-charge odd crystal-field components and the low-lying ligand-field states is in poor agreement with experiment, suggesting that odd vibrations play an important role in the observed intensity. A band found at 11 200 cm^{-1} in iron-doped Al_2O_3 is attributed to Fe^{2+}, whose presence was confirmed by the Mössbauer technique.

ACKNOWLEDGMENTS

The authors wish to express their thanks to R. A. Becker for growing the flux-grown crystals used, to C. S. Sahagian for the Verneuil crystals, to D. W. Forester for a Mössbauer analysis, and to E. J. Brooks for x-ray-fluorescence and chemical analyses. We also wish to thank F. De S. Barros for a preprint of their work.

APPENDIX: ELECTRIC DIPOLE MATRIX ELEMENTS

The ith component of the electric dipole matrix element between cubic crystal-field states may be written as

$$\langle P(i) \rangle = \langle S\Gamma M\gamma | P(i) | S'\Gamma'M'\gamma' \rangle \ . \qquad \text{(A1)}$$

Since we are interested in transitions between states of the same parity and different spin, the spin-orbit interaction and odd crystal fields are invoked to permit these transitions. This leads to the following matrix element between states a and b:

$$\langle P(i)\rangle = \sum_{l,n} \langle a|\, V_{\text{odd}}\,|c^l\rangle\langle c^l|\, P(i)\,|d^n\rangle\langle d^n|\, V_{s\text{-}o}\,|b\rangle \times [\Delta(a,c^l)\Delta(b,d^n)]^{-1} + \sum_{l,n} \langle a|\, P(i)\,|c^l\rangle\langle c^l|\, V_{\text{odd}}\,|d^n\rangle\langle d^n|\, V_{s\text{-}o}\,|b\rangle \times [\Delta(b,c^l)\Delta(b,d^n)]^{-1} + \text{other permutations}\ , \quad \text{(A2)}$$

where

$$\Delta(a,b) = E(a) - E(b)\ , \quad \text{(A3)}$$

and states labelled l are ligand states, the other states being essentially central-ion states.

It is necessary to consider the various terms in Eq. (A2) in detail. Thus the dipole-operator components $P(i)$ transform like components of T_{1u} of O_h. The index takes on the values 0 and ± 1, and for linearly polarized light in a trigonal system, the components of P of interest are

$$P_{\parallel} = P(0)\ , \qquad P_{\perp} = (2)^{-1/2}[|P(1)|^2 + |P(-1)|^2]^{1/2}\ . \quad \text{(A4)}$$

The odd crystal field due to point charges is given by

$$V_{\text{odd}} = B_1^0 r\cos\theta + B_3^0 r^3(5\cos^3\theta - 3\cos\theta) + B_3^3 r^3\sin^3\theta\cos 3\varphi + C_3^3 r^3\sin^3\theta\sin 3\varphi = V_1(T_{1u})r + V_3(T_{1u})r^3 + V(A_{2u})r^3 + V(T_{2u})r^3\ , \quad \text{(A5)}$$

where the axis of quantization is the [111] direction. The first grouping is due to McClure[8] and defines the crystal-field sums B_i^m while the second grouping illustrates how various odd components of the crystal field transform in O_h. The first three terms transform as A_1 in both C_{3v} and C_3 while the last term transforms as A_2 in C_{3v} and A_1 in C_3. Explicit expressions for the various V terms can be found in Artman and Murphy.[32] It should be noted, however, that $V(T_{2u})$ is proportional to C_3^3.

Finally, the spin-orbit operator $V_{s\text{-}o}$ may be written as

$$V_{s\text{-}o} = \sum_i \zeta_i \vec{l}_i\cdot\vec{s}_i = \sum_{q\bar{\gamma}} a_{q\bar{\gamma}} \sum_i s_{iq} t_{i\bar{\gamma}}\ , \quad \text{(A6)}$$

using the notation of Tanabe and Kamimura.[37] Here s_{iq} transforms as the components of $D^{(1)}$ in the spin-rotation group and $t_{i\bar{\gamma}}$ transforms as T_{1g} of O_h. Note that the $a_{q\bar{\gamma}}$ parameters are nondimensional in this formulation.

Consider now a transition between the ground-state component $|\frac{5}{2}A_1 M'\gamma'\rangle$ and the excited state $|\frac{3}{2}\Gamma M\gamma\rangle$ of Fe^{3+}. We assume that the spin-orbit interaction is negligible except between the predominantly Fe^{3+} states.[5] This eliminates all but the first two sums in Eq. (A2), and the method of irreducible tensor operators[38] is then applied using Eqs. (A4)–(A6) to yield

$$\langle \tfrac{3}{2}\Gamma M\gamma|\, P(i)\,|\tfrac{5}{2}A_1 M'\gamma'\rangle = \sum V\begin{pmatrix}\Gamma & \Gamma_k^l & \Gamma_j^u\\ \gamma & \gamma_k & \gamma_j\end{pmatrix} V\begin{pmatrix}\Gamma_k^l & \Gamma_4^n & \Gamma_4^u\\ \gamma_k & \gamma_4 & i\end{pmatrix}\sum_{q\bar{\gamma}} a_{q\bar{\gamma}}\,\overline{V}\begin{pmatrix}\frac{3}{2} & \frac{5}{2} & 1\\ -M & M' & q\end{pmatrix} \times V\begin{pmatrix}\Gamma_4^n & A_1 & \Gamma_4\\ \gamma_4 & q & \bar{\gamma}\end{pmatrix}(-1)^{k+1+S-M}\langle\Gamma\|\,\Gamma_j^u\,\|\Gamma_k^l\rangle\langle\Gamma_k^l\|\,P\,\|\Gamma_4^n\rangle\langle\Gamma_4^n\|\,\Gamma_4\,\|{}^6A_1\rangle[\Delta({}^6A_1, {}^4T_1^n)\Delta(\Gamma,\Gamma_k^l)]^{-1} + \cdots\ . \quad \text{(A7)}$$

Here Γ_j^u is the representation of a component of V_{odd} and the double-barred elements are reduced matrices. Note that the spin-orbit operator can mix only ${}^4T_1$ states with ${}^6A_1$.

Because the various components of the ${}^6A_1 \rightarrow {}^4A_1$ band are not resolved, we consider the value of P^2 summed over all components. When one carries out the algebra, one obtains

$$|\langle {}^4A_1|\, P(\parallel)\,|{}^6A_1\rangle|^2 = \tfrac{4}{27}\zeta^2\left(\sum_{l,n}\sigma_n V'[T_2^l, T_2]P'[T_2^l, T_1^n]\right)^2\ , \quad \text{(A8)}$$

$$|\langle {}^4A_1|\, P(\perp)\,|{}^6A_1\rangle|^2 = \tfrac{1}{9}\zeta^2\left(\sum_{l,n}\sigma_n V'[T_1^l, T_1]P'[T_1^l, T_1^n] + (\sigma_n/\sqrt{3})V'[T_2^l, T_2]P'[T_2^l, T_1^n]\right)^2\ , \quad \text{(A9)}$$

where

$$\sigma_n = [\sqrt{2}(\lambda_n + \nu_n) + \mu_n][\Delta({}^6A_1, {}^4T_1^n)]^{-1}$$

and λ_n, μ_n, and ν_n are the coefficients of the various d^5 configurations which make up ${}^4T_1^n$, as given by Koide and Pryce.[33] Further, we have

$$V'[T_i^l, T_j] = \langle {}^4A_1\,\|\,V(T_j)\,\|{}^4T_i^l\rangle[\Delta({}^4A_1, {}^4T_i^l)]^{-1}\ ,$$

$$P'[T_i^l,\ T_1^n] = \langle {}^4T_i^l\,\|\,P\,\|\,{}^4T_1^n\rangle\ .$$

The radial integrals $\langle r^n\rangle$ and $\langle r\rangle$, arising from

the potential and electric dipole operators, respectively, have been suppressed in the above equations, but they are used in the text in the numerical evaluation of the oscillator strengths.

[1]K. H. Wickersheim and R. A. Lefever, J. Chem. Phys. 36, 844 (1962).

[2]D. L. Wood and J. P. Remeika, J. Appl. Phys. 38, 1038 (1967).

[3]A. J. Kurtzig, R. Wolfe, R. C. Lecraw, and J. W. Nielsen, Appl. Phys. Letters 14, 350 (1969).

[4]A. J. Kurtzig and H. J. Guggenheim, Appl. Phys. Letters 16, 43 (1970).

[5]F. J. Kahn, P. S. Pershan, and J. P. Remeika, Phys. Rev. 186, 891 (1969).

[6]N. T. Melamed, P. C. Viccaro, J. O. Artman, and F. De S. Barros, J. Luminescence 1/2, 348 (1970); and private communication.

[7]R. G. Wyckoff, *Crystal Structure* (Interscience, New York, 1948), Vol. II.

[8]D. S. McClure, J. Chem. Phys. 36, 2757 (1962). This reference summarizes many useful details concerning the optical absorption of transition-metal ions in Al_2O_3.

[9]J. J. Krebs, Phys. Rev. 135, A396 (1964).

[10]V. J. Folen, Phys. Rev. 125, 1581 (1962); J. W. Nielsen and E. F. Dearborn, J. Phys. Chem. Solids 5, 202 (1958).

[11]K. Moorjani and N. McAvoy, Phys. Rev. 132, 504 (1963).

[12]M. G. Townsend, Solid State Commun. 6, 81 (1968).

[13]G. Lehmann and H. Harder, Am. Mineralogist 55, 98 (1970).

[14]Y. Tanabe and S. Sugano, J. Phys. Soc. Japan 9, 753 (1954).

[15]R. Stevenson, *Multiplet Structure of Atoms and Molecules* (Saunders, Philadelphia, Pa., 1965).

[16]W. Low and G. Rosengarten, J. Mol. Spectry. 12, 319 (1964).

[17]K. A. Schroeder, J. Chem. Phys. 37, 1587 (1962).

[18]D. H. Goode, J. Chem. Phys. 43, 2830 (1965).

[19]Y. Shadmi, quoted in Ref. 16.

[20]S. Geschwind and J. P. Remeika, J. Appl. Phys. 33, 370 (1962).

[21]R. Englman, Mol. Phys. 3, 183 (1961).

[22]C. Moore, *Atomic Energy Levels*, Natl. Bur. Std. Circ. No. 467 (U. S. GPO, Washington, D.C., 1952), Vol. II.

[23]A. M. Clogston, J. Appl. Phys. 31, 198S (1960); H. H. Tippins, Phys. Rev. B 1, 126 (1970).

[24]A. L. Schawlow, D. L. Wood, and A. M. Clogston, Phys. Rev. Letters 3, 271 (1959).

[25]J. Ferguson, H. J. Guggenheim, and Y. Tanabe, J. Appl. Phys. 36, 1046 (1965).

[26]J. Ferguson, H. J. Guggenheim, and Y. Tanabe, Phys. Rev. Letters 14, 737 (1965).

[27]J. Ferguson, H. J. Guggenheim, and Y. Tanabe, J. Phys. Soc. Japan 21, 692 (1966).

[28]J. Ferguson, Solid State Commun. 5, 773 (1967); Australian J. Chem. 21, 307 (1968).

[29]W. Trifthäuser and D. Schroeer, Phys. Rev. 187, 491 (1969).

[30]Crystals supplied by C. S. Sahagian, Air Force Cambridge Research Laboratories, Bedford, Mass.

[31]D. S. McClure, in *Solid State Physics*, edited by F. Seitz and D. Turnbull (Academic, New York, 1959), Vol. 9.

[32]J. O. Artman and J. C. Murphy, Phys. Rev. 135, A1622 (1964).

[33]S. Koide and M. H. L. Pryce, Phil. Mag. 3, 607 (1958).

[34]A. S. Barker, Jr., Phys. Rev. 132, 1474 (1963).

[35]S. P. S. Porto and R. S. Krishnan, J. Chem. Phys. 47, 1009 (1967).

[36]I. Adams, J. W. Nielsen, and M. S. Story, J. Appl. Phys. 37, 832 (1966).

[37]Y. Tanabe and H. Kamimura, J. Phys. Soc. Japan 13, 394 (1958).

[38]J. S. Griffith, *The Irreducible Tensor Method for Molecular Symmetry Groups* (Prentice-Hall, Englewood Cliffs, N. J., 1962).

PHYSICAL REVIEW B VOLUME 4, NUMBER 3 1 AUGUST 1971

Theoretical Estimates of the Isotropic hfs Constants of Small Ions in the Neighborhood of a Massive Ion with an Unpaired Electron*

Supriya Ray

Chemistry Division, Argonne National Laboratory, Argonne, Illinois 60439

(Received 15 December 1970)

Estimates of the isotropic part of the hyperfine constants of several small ions in the presence of a massive ion with an unpaired electron, by the use of a simple method, are reported here. Calculated results are found to be quite essential in the understanding of isotropic hfs observed in similar systems in the crystal environment.

I. INTRODUCTION

Considerable attention has been focused in recent years on the use of paramagnetic-resonance spectra and optical spectra to detect impurity centers in x-irradiated α (low)-quartz.[1,2] As a substituent for silicon in the quartz lattice, germanium (as well as a few other elements, including aluminum,